Available online at www.sciencedirect.com

ScienceDirect

journal homepage: www.elsevier.com/locate/he

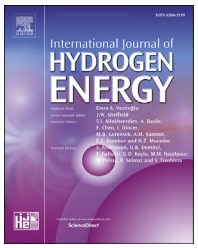

The relationship between chemical structure of perfluorinated sulfonic acid ionomers and their membrane properties for PEMEC application

Jun Hyun Lim [a,1], *Jian Hou* [a,1], *Woo Young Kim* [a], *Sungsool Wi* [b], *Chang Hyun Lee* [a,*]

[a] *Department of Energy Engineering, Dankook University, Chungnam 31116, Republic of Korea*
[b] *National High Magnetic Field Laboratory, Florida State University, Tallahassee, FL 32310-3706, USA*

HIGHLIGHTS

- PFSA ionomers of the various types of chemical structures and equivalent weights that serve as PEM materials for PEMEC are studied.
- The relationships between the chemical structures of PFSA ionomers and the dispersion characteristics as well as the membrane properties were examined.
- The membranes derived from shorter side-chain PFSA ionomers exhibited improved gas barrier and proton conductivity properties.

ARTICLE INFO

Article history:
Received 23 July 2023
Received in revised form
4 September 2023
Accepted 12 September 2023
Available online 26 September 2023

Keywords:
Perfluorinated sulfonic acid (PFSA) ionomers
Polymer electrolyte membrane (PEM)
Water electrolysis
Chemical architecture
Solid-state ^{19}F NMR

ABSTRACT

Polymer electrolyte membrane electrolyzer cells (PEMECs) has been confirmed as a prototype electrochemical system that is effective in converting water into hydrogen and oxygen under the application of electricity. Among the core components of PEMEC, the polymer electrolyte membrane (PEM) determines critically an overall electrochemical performance of the PEMEC. Ideally a PEM system should exhibit a complex transport behavior of small molecules (e.g., gases and ions) while mediating flows of ions in the cell; it should exhibit high proton selectivity while serving as a gas barrier to hydrogen and oxygen to increase current efficiency, which are in turn vital factors in determining an effectiveness when the electric energy is used for water electrolysis. Until now, perfluorinated sulfonic acid (PFSA) ionomers have been extensively used as PEM materials in water electrolysis while in generating hydrogen and oxygen gases simultaneously in high purity. In this study we have examined the chemical structure of PEM membranes derived from various types of PFSA ionomers by employing solid-state ^{19}F MAS NMR. Subsequently, a structure-property-performance correlation was sought in accordance with the chemical structure, the dispersion characteristics, and membrane properties of PFSA ionomers. Furthermore, the effects of the membrane morphology as well as the ionomer packing characteristics on proton conduction and hydrogen transportation were investigated. Lastly, the membrane properties exerted by varying the chemical architectures and equivalent weight (EW) values of PFSA ionomers in PEMEC were confirmed. 3 M 725 membrane, which has the highest concentration of sulfonic acid groups in the hydrated

* *Corresponding author.*
E-mail address: chlee@dankook.ac.kr (C.H. Lee).
[1] These authors contributed equally to this work.
https://doi.org/10.1016/j.ijhydene.2023.09.131

state, has the highest proton conductivity. In addition, it showed the best water electrolytic cell performance via the synergistic effect with low gas permeability obtained as a result from the short side chain structure.

1. Introduction

Hydrogen (H_2) as a clean fuel has gotten a lot of attention around the world as an alternative to fossil fuels. The gaseous H_2 has the lowest volumetric basis energy density (0.3 kWh/L@25 °C and 135 atm) and the highest weight basis energy density (27.1 kWh/kg) among currently available fuels. Thus, it is necessary to compress H_2 gas for guaranteeing a long-distance journey per fueling in the hydrogen electric vehicles [1–4].

PEMEC (polymer electrolyte membrane electrolytic cell) has been reported as one of the representative approaches responsible for producing high-purity H_2 gas [1,4]. A PEMEC consists of an anode, a cathode, a polymer electrolyte membrane (PEM), catalyst layers, bipolar plates, and so forth [5,6]. To be more specific, a PEM in PEMEC serves as the vital component in determining the electrochemical performance along with electrode materials [7,8]. In general, a PEM should satisfy to the required characteristics, such as high proton conductivity, mechanical, chemical and thermal stabilities, and low gas permeability, etc.

The development of an ideal type of membrane materials for PEMEC, while fulfilling all above-mentioned requirement, is under subject to the numerous technical obstacles in real applications [9,10]. An extensive research on this matter has shed a clue that the molar ratio of H_2 to O_2 produced in PEMEC is 2 to 1, and when a difference exists in this ratio, it causes a significant pressure variation that arises between the anode and cathode electrodes that are in direct contact with PEM [11]. As the pressure of the H_2 gas generated by the PEMEC system rises, it turned out that this H_2 to O_2 pressure difference also increases. Moreover, the penetration of H_2 gas into PEM can trigger a serious safety problem, such as an explosion, when H_2 reacts with O_2 [12,13].

Perfluorinated sulfonic acid (PFSA) ionomers possess high oxidative and mechanical stability under harsh conditions, high proton conductivity, and electrochemical durability. For this reason, PFSA ionomers have been exclusively utilized as a PEM material thus far [14,15]. Specifically, Nafion® membranes derived from the perfluorinated ionomers have been considered as a benchmark material in PEMEC systems because of its prominent chemical stability and performance [16–18]. However, the Nafion® membrane system has shown highly permeable H_2 gas due to the presence of $-CF_3$ groups in the side chains. This high permeability of H_2 easily triggers an increase in ohmic potentials at a fixed current density and a reduction in hydrogen production at a constant power density, thereby resulting in a direct loss in the efficiency of PEMECs and more energy consumption [19]. Additionally, H_2 gas crossover through the membrane would result in chemical degradation of the PFSA ionomer membrane because of the formation and migration of hydrogen peroxide and hydroperoxyl radicals that attack all H-containing end bonds present in the ionomers [20].

To solve these problems associated with fast H_2 permeation frequently observed in Nafion® membrane, called as a long-side chain PFSA membrane, there have been trials to shorten the side chain length [21] which are known as short-side chain PFSA ionomer membrane researches. They include the removal of vulnerable structural parts (e.g., swivel ether group) to such radical attacks. Different in general polymers whose structural modification can be examined readily by liquid NMR analysis, a poor solubility of the PFSA ionomer in organic solvents makes liquid NMR experiment difficult. To address this problem, the chemical structure of the PFSA ionomer was analyzed by employing solid-state ^{19}F MAS NMR experiment.

In this study, PFSA ionomers with various types of chemical structures (e.g., long-side chain vs. short-side chain) and equivalent weights (EWs) were used as PEM materials for PEMEC. The correlations found between chemical structures of PFSA ionomers and the dispersion characteristics as well as the membrane properties are fully discussed. Furthermore, the effects of membrane morphology and ionomer packing on proton conduction and H_2 gas transport behavior were investigated. Finally, the effects of chemical structures and equivalent weights of PFSA ionomers on the membrane properties for PEMEC has been provided. To date, there have been no scientific papers which systematically deal with the influences of chemical structures and EW values of PFSA ionomers on membrane characteristics including electrochemical performances.

2. Materials and methods

2.1. Materials

Nafion (NR) emulsion D2021 (EW = 1100 g/eq) (DuPont, Wilmington, DE, USA) and Aquivion (AQ) ionomer powders (EW = 720, and 790 g/eq) (Solvay, Brussels, Belgium) were purchased from Sigma-Aldrich Ltd. (WI, USA). 3 M ionomer powders (EW = 725, and 800 g/eq) were from 3 M Advanced Materials Division, USA. The 1-propanol solvent was purchased from Sigma-Aldrich Ltd. (WI, USA) and used as received. Each PFSA ionomer sample is denoted as the abbreviation of the ionomer_EW value, irrespective of their state (e.g., dispersion or membrane). Moreover, each sample is clearly distinguished by the state in which characterization is performed.

2.2. PFSA ionomer characterization

The chemical structures of the PFSA ionomers were characterized by solid-state ^{19}F MAS NMR spectroscopy conducted at the National High Magnetic Field Laboratory (NHMFL) in USA. The NMR experiments were carried out in a 14.1 T wide bore magnet solid-state NMR spectrometer that is operated by the Bruker Avance III console while using a Bruker's ^{1}H-X-Y 1.3 mm MAS probe. The ^{1}H channel was tuned to ^{19}F frequency for the experiment. Each PFSA sample in solid form was packed into a 1.3 mm MAS rotor, and the rotor was spun at 40 kHz MAS rate for the experiment. A single 2 μs rf pulse was used to cover a wide frequency range of the chemical shift anisotropy of ^{19}F peaks with about ~100 kHz power to record ^{19}F MAS NMR peaks. ^{19}F MAS NMR peaks were assigned according to the literature [22] and were integrated to quantify each ^{19}F site while coadding the intensities arising from the spinning sidebands to the main peaks [23,24].

The thermal stability of the PFSA ionomers was determined by TGA (PYRIS 1 TGA, Perkin Elmer, USA). The samples were pre-heated in a nitrogen atmosphere from an ambient temperature to 90 °C at a rate of 10 °C/min in 30 min and then cooled back to 30 °C for the removal of the absorbed moisture prior to the respective test. TGA analysis was performed under two modes:1) heating mode [25] and 2) isothermal mode. Under the heating mode, the TGA measurement was carried out in the temperature range from 30 °C to 600 °C at the rate of 10 °C/min. For the isothermal mode, the weight variation was analyzed while maintaining the temperature for 2 h after raising the temperature from 30 °C to 200 °C, 250 °C, and 300 °C, respectively. Furthermore, the thermal degradation behaviors of the ionomers were monitored by examining the weight loss of the samples as a function of temperature.

2.3. Dispersion characterization

The viscosity of 4 wt% of the PFSA ionomer dispersions was examined using a digital viscometer (DV2TLVJ0, Brookfield, USA) in accordance with the ASTM D2196. A small sample adapter was operated to accurately measure the viscosity of small samples at various shear rates at 25 °C by regulating the spindle rotational speed at 10 and 40 s^{-1}, respectively [20]. The particle size of the PFSA ionomers in aqueous 1-propanol (water: 1-propanol = 55: 45 wt%) [26] was analyzed with the dynamic light scattering instrument (DLS, Model Zetasizer Nano ZS, Malvern, Worcestershire, UK) at 25 °C. The concentrations of the PFSA-dispersed solutions were regulated at 0.01 wt% [27,28].

2.4. Membrane fabrication and acidification

A PFSA-dispersed solution of either 3 M or AQ ionomer powders was prepared by stirring the sample in a mixed solution of water and 1-propanol (water: 1-propanol = 55 : 45 wt%) for 48 h [28]. Each ionomer colloidal solution was casted on a glass slide to fabricate a membrane film by following the known solution-casting method [29,30], which was then dried at 85 °C for 8 h, heated to 100 °C for 15 min and 190 °C for 12 min in a vacuum oven. The resulting membrane was gently removed from the glass plates in deionized water, which was subsequently immersed in a boiling solution of 0.5 M H_2SO_4 for 2 h. This acidified membrane was washed in boiling water for another 2 h to thoroughly remove the residual H_2SO_4 [31–33]. The thickness value of the resulting membranes was around 50 ± 1 μm in the dry state. All the membranes were kept in a vacuum oven prior to further characterization.

2.5. Membrane characterization

The small-angle X-ray scattering (SAXS) patterns were generated using a 4 C SAXS II beamline with 3.0 GeV power available at Pohang Accelerator Laboratory II (PAL II) in South Korea. An X-ray wavelength of 0.07 nm was generated with a beam flux of 1×10^{12} ph/s and a beam size of 100 (V) × 300 (H) μm^2 using the SAXS instrument. The sample-to-detector distance was fixed at 1 m. The interdomain distance was obtained in accordance with Bragg's law [34,35]. Field-emission transmission electron microscopy (TEM, LIBRA® 120, Carl Zeiss, Oberkochen, Germany) was carried out to obtain visualized morphological information of the PFSA membranes. For this, all the samples were stained with a 2 wt% lead acetate solution.

The resistance of each membrane sample (1.0 cm × 4.0 cm) was examined with a Pt electrode connected with multichannel potentiostat (VMP3, Biologic, France) based on a 4-probe alternating current (AC) impedance under a wetting condition at variously controlled temperatures (e.g., 30, 45, 60, 75, and 90 °C). The proton conductivity was then calculated according to the following equation, **Eq. (1)**: [36]

$$\sigma\left(\frac{S}{cm^2}\right) = \frac{l}{R \times S}$$

where σ is proton conductivity, R is ohmic resistance, l is distance between electrodes, and S is cross-sectional area of the membrane.

The sulfonic acid concentration in a unit volume was examined in accordance with the volume-based ion exchange capacity specified in the hydrated state ($IEC_{v(wet)}$). The weight-based IEC (IEC_w) was examined through the conventional titration (ASTM D2187) method while obtaining $IEC_{v(wet)}$ as written by the following equation, **Eq. (2)**: [37,38]

$$IEC_{v(wet)}\ (meq/cm^3) = \frac{(IEC_w \times \delta_d)}{(1 + 0.01 \times WU)}$$

where δ_d denotes the density of membrane in the dry state and WU is the amount of water uptake.

The density of a dried membrane was obtained after treating the membrane at 60 °C for 24 h in a vacuum oven. Subsequently, the membrane was immersed in deionized water for 24 h to secure a wet condition. The dried and wet densities of a membrane (dimension = 5.0 cm × 5.0 cm) were determined by using **Eq. (3-4)**:

$$Dry\ density\ (g/cm^3) = W_{dry}/V_{dry}$$

$$Wet\ density\ (g/cm^3) = W_{wet}/V_{wet}$$

where V_{wet} and V_{dry} denote the volume of wet and dried membrane, respectively, and W_{wet} and W_{dry} represent the weights of wet and dried membrane, respectively.

The water uptake of membranes (dimension = 5.0 cm × 5.0 cm) was determined by comparing the weight difference between the dried and wet states. The water uptake of the membranes was then determined by weight percentage using the following equation, **Eq. (5)**:

$$Water\ uptake\ (\%) = \frac{(W_{wet} - W_{dry})}{W_{dry}} \times 100,$$

where W_{wet} and W_{dry} designate the weights of wet and dried membranes.

The tensile strength of a membrane was examined by using a universal testing machine (UTM, T7000 M, Korea Measurement & Testers (KMT), Korea) in accordance with the ASTM D882 while employing a cross head speed of 10 mm/min [39].

The alpha transition temperature (T_α) of PFSA ionomers was determined by using a dynamic mechanical analyzer (DMA, DMA 8000, Perkin Elmer Corp., USA) at a ramp speed of 5 °C/min from 30 °C to 300 °C under 1 atm [40,41].

The gas permeability coefficient of a membrane was determined by varying the temperature using the time-lag method [42]. The time-dependent variation of the pressure was measured in an evacuated lower chamber by reading a pressure sensor (Baratron®, MKS, USA) that possesses a sensitivity in the range of 10^{-3} cm Hg. The gas permeability coefficient P in Barrer (10^{10} cm^3_{stp} cm/sec cm^2 cm Hg) was determined by using the following formula given as **Eq. (6)**: [43,44]

$$P\ (Barrer) = \frac{V_b \times l}{p_a \times A \times R \times T} \times \frac{dp_b}{dt}$$

where V_b denotes the volume of the lower chamber in cm^3, l is the membrane thickness in cm, A is the exposed surface area of the membrane in cm^2, T is temperature in K, p_a is the pressure of the upper chamber in cm Hg, R is the gas constant (6236.367 cm Hg cm^3/mol K), and dp_b/dt is the rate of the pressure variation in time that is measured in the linear part of the pressure-time curve (cm Hg/sec).

2.6. PEMEC performance evaluation

In preparing a membrane electrode assembly (MEA), a cathode catalyst ink slurry was prepared by using a commercially available Pt/C catalyst system (40 wt%, Johnson Matthey, USA). The resulting ink slurry was coated onto the cathode side of the synthesized membranes by employing a spray method for cathode formation. The anode ink slurry was also prepared in a similar manner, except using an IrO_2 catalyst system (BOYAZ ENERGY, Korea). The ink slurry was sprayed onto the opposite side of an identical membrane. The loaded amount of Pt/C and IrO_2 catalysts on the membrane surfaces had reached 0.4 mg/cm^2 and 2 mg/cm^2, respectively. Subsequently, a MEA was assembled in a single cell with an active area of 9 cm^2. To activate the MEA, deionized water was flown to the anode at 80 °C at the rate of 10 sccm for 2 h. A current-voltage polarization curve was generated at 80 °C by using a potentiostat (HCP 803, Biologic, France).

3. Results and discussion

3.1. Structure identification by solid-state ^{19}F MAS NMR

Solid-state ^{19}F MAS NMR experiments were conducted for the structural analysis of the PFSA ionomers while utilizing an ultrafast MAS rate (40 kHz) to minimize the spinning sidebands. Solid-state MAS NMR method must be employed for the analysis of the PFSA ionomers because these ionomers are insoluble in organic solvents. Fig. 1 shows thus measured solid-state ^{19}F MAS NMR spectra of PFSA ionomers that are commercially available. PFSA ionomers consist of poly(tetrafluoroethylene) main chain and perfluorinated side chains that possess $-SO_3H$ groups at the terminal ends. The ^{19}F NMR spectrum of the Nafion exhibits the presence of branched $-CF_3$ as well as ether (-O-) groups in the side chains. It is reported that these tertiary fluorine CF_3-C-F and ether (-O-) groups in the side chains are responsible for in lessening the compact packing of ionomer chains, resulting in a relatively low chemical durability of the Nafion [45,46]. These peaks are absent in the ^{19}F MAS NMR spectra of other PFSA ionomers as expected. The chemical structure of 3 M ionomers confirmed by ^{19}F MAS NMR spectra indicates that there are four-connected carbon (C4) structures in their side chains regardless of the EW values. Moreover, when the ^{19}F MAS NMR spectra of other ionomers were inspected, two-connected carbon (C2) structures were identified in the structure of AQ ionomers with an additional small peak at −110 ppm when AQ

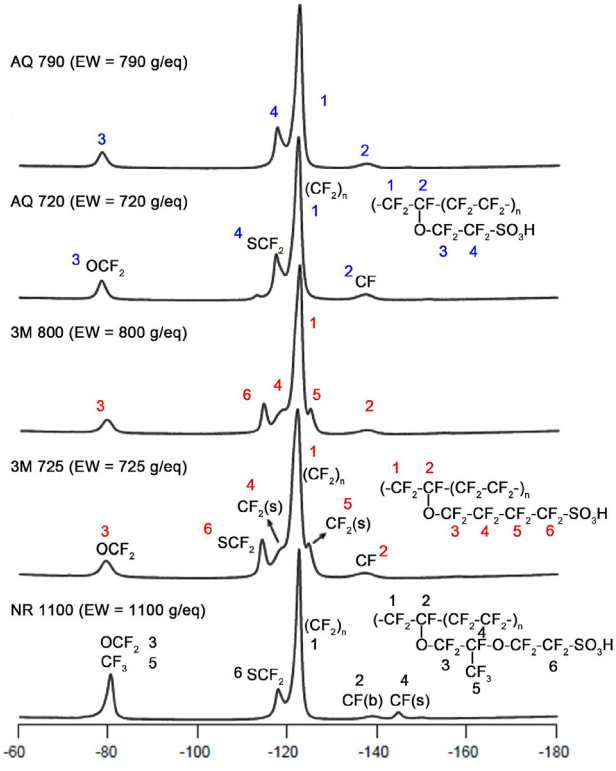

Fig. 1 – Solid-state ^{19}F MAS NMR spectra of various types of PFSA ionomers in the membranes.

720 is used. According to this observation, the AQ 720 type ionomers consist mostly of the C2 structures rather than three-connected carbon (C3) structures [47,48].

3.2. *Thermal degradation behavior*

The thermal stability of the PFSA ionomers was examined by TGA as shown in Fig. 2 (a). All the PFSA ionomers displayed a three-step weight loss pattern as the temperature varies. The first weight loss (Region I) occurred broadly from ~100 °C to 180 °C as the water molecules in the PFSA ionomers are removed [49]. The second weight loss (Region II) occurs at 225 °C that might be correlated to the thermal decomposition of sulfonic acid groups: the sulfonic acid contents in the PFSA ionomers decrease as a function of their EW values [20]. The last weight loss (Region III) that occurs at the temperature range over 420 °C might be correlated to the thermal degradation of perfluorinated backbone and side chains [49,50].

Fig. 2 (b)–(d) illustrates the thermal resistance of the PFSA ionomers obtained at three different temperatures (200, 250, and 300 °C) of the TGA thermograms. This analysis evaluates the degradation extent of the sulfonic acid groups in each PFSA ionomer type under constant temperature conditions. The theoretical sulfonic acid content was determined based on each EW value and compared to the weight loss (m_{loss}) at each examined temperature. An influence of the potentially existing small quantity of strongly bound water was excluded in our analysis. It seems like that all the PFSA ionomers considered in our study were thermally stable near 200 °C for 2 h. In temperature ranges higher than 250 °C, 3 M ionomers maintain excellent thermal resistances without a noticeable loss of sulfonic acid groups (<3.5% of total sulfonic acid content), but C2 ionomers, particularly the AQ sample, showed a loss of about 9–12%. This observation is congruent to the theoretically calculated sulfonic acid contents. A noticeable loss in the amount of sulfonic acid groups could result in a critical reduction in the proton transport property [28]. Nonetheless, the thermal stability of the C2 ionomers seems to be superior to that of NR 1100.

3.3. *Dispersion characteristics*

The dispersion characteristics of the PFSA ionomers are summarized in Table 1. Except AQ ionomers, all the other types of PFSA ionomers do not show any meaningful variations in the viscosity as the shear rate varies. Thus, as judged by this result, ionomer particles are homogeneously dispersed in the mixed solution of water and propanol, maintaining a

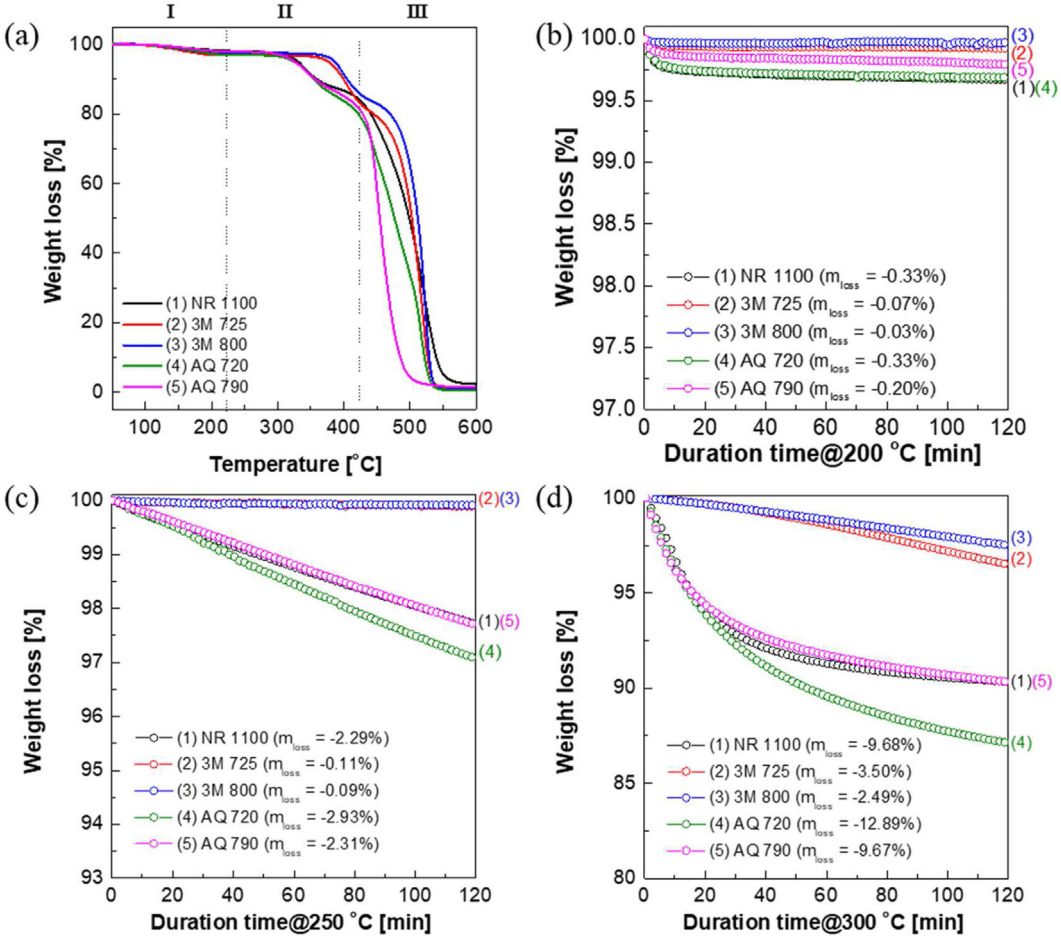

Fig. 2 – Thermal degradation behavior of the PFSA ionomers (a) under the heating mode in N_2 atmosphere, at (b) 200 °C, (c) 250 °C, and (d) 300 °C under the isothermal mode in N_2 atmosphere using thermogravimetric analyzer.

Table 1 – Fundamental characteristics of PFSA ionomers.

PFSA dispersion	Viscosity [cP][a]		Average particle size[b] [nm]
	Share rate = 10/sec	Share rate = 40/sec	
NR 1100	23.3	19.2	3.78 ± 0.43
3 M 725	22.1	19.0	2.23 ± 0.22
3 M 800	15.4	12.2	3.23 ± 0.32
AQ 720	NA	NA	2.17 ± 0.09
AQ 790	105.8	71.1	3.50 ± 0.58

[a] Examined with PFSA dispersion diluted to an ionomer concentration of 4 wt%.
[b] Examined using dynamic light scattering (DLS, Zetasizer Nano ZS, Malvern, Worcestershire, UK) analysis.

stable dispersion phase. To be more specific, under the environment of possessing strong hydrogen bonds between sulfonic acid groups and hydrophilic solvent molecules, the 3 M ionomers with low EW values would exhibit increased values in the viscosity. The extent of dispersions of the AQ samples was noticeable. For instance, the viscosity of the dispersed solution of the AQ 720 was extremely high even at the concentration of about 4 wt%, resulting in an unmeasurable shear rate.

The average particle size of ionomers dispersed in aqueous alcohol media should be reduced because small ionomer particles may induce compactly packed membrane structures, which can retard H_2 passage [29]. Under the presence of bulky $-CF_3$ groups in the side chains, the dispersion of Nafion ionomers in the mixed solution would form a relatively large average particle size. Previous research results suggested that the dispersed ionomer particles of short-side chain (SSC) ionomers (e.g., 3 M and AQ ionomers) exhibit a slightly smaller average particle size than that of Nafion ionomers [51]. The particle size of the SSC ionomers is proportional to the EW values. The smallest average ionomer particle sizes were identified from the 3 M 725 and AQ 720 dispersions.

3.4. *Membrane characteristics*

One of the critical properties of membranes employed in PEMEC is the proton conductivity that can correspond the slope in the ohmic polarization region of the electrochemical PEMEC performance curve. In general, a less steep slope in the region, a higher proton conductivity in the membrane is expected. The proton conductivity is often influenced by the morphology of membranes [52]. The morphology of ionomer membranes was examined using the small angle X-ray scattering (SAXS) technique with an irradiation angle of 90°. Fig. 3 shows SAXS patterns of the PFSA ionomer membranes thus obtained in which the spatial arrangement of hydrophilic domains was examined to be perpendicular to the membrane plane. All the PFSA ionomer membranes possess strong scattering maxima (e.g., q_{max} and $2q_{max}$) because of having ionic aggregations in their hydrophilic domains. The ratio of $2q_{max}$ to q_{max} generally approaches to 2 (Table 2). It suggests that all the PFSA ionomer membranes exhibit lamellar morphologies composed of hydrophilic and hydrophobic domains regardless of their chemical architectures [53,54]. The lamellar

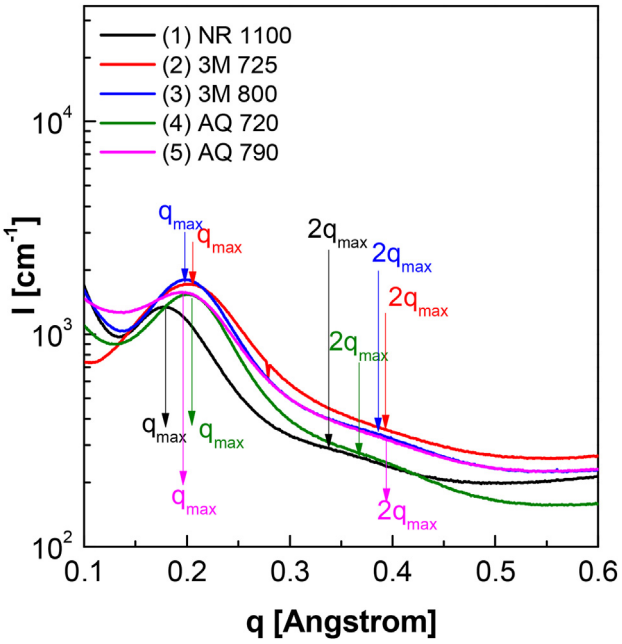

Fig. 3 – SAXS profiles of PFSA ionomer membranes.

morphologies turned out to be clearly distinctive, presumably due to possessing an improved hydrophilic-hydrophobic microphase separation. The hydrophilic-hydrophobic microphase separation increases when the hydrophilicity increases, or the EW value decreases. Furthermore, the ratio of $2q_{max}$ to q_{max} approaches to 2 even in the case of PFSA ionomer membranes (e.g., 3 M 725 and AQ 720) that possess a relatively low EW value.

The q_{max} scattering peaks of the SSC-PFSA ionomer membranes are positioned in higher q vector direction as compared to that of NR 1100 [55]. This characteristic can be explained by the interdomain distance presented in Table 2 (i.e., the average distance between their hydrophilic domains). It is noteworthy that the interdomain distances existing in the SSC-PFSA ionomer membranes are shorter than those from the long-side chain (LSC) ionomer membranes. This trend is consistent with that in observed in TEM images of NR 1100 and 3 M 725 (Fig. 4). The distance between hydrophilic domains marked in dark color is narrow in 3 M 725, while the hydrophilic domains of NR 1100 are widely

Table 2 – Morphological information of the PFSA ionomer membranes on the basis of their SAXS profile.

PFSA membrane	Interdomain distance[a] [nm]	q_{max} [Å^{-1}]	$2q_{max}$ [Å^{-1}]	$2q_{max}/q_{max}$
NR 1100	3.51	0.179	0.335	1.87
3 M 725	3.13	0.200	0.394	1.97
3 M 800	3.16	0.199	0.385	1.93
AQ 720	3.12	0.201	0.399	1.99
AQ 790	3.21	0.196	0.367	1.86

[a] Obtained via theoretical conversion using Bragg's law with each q_{max} value.

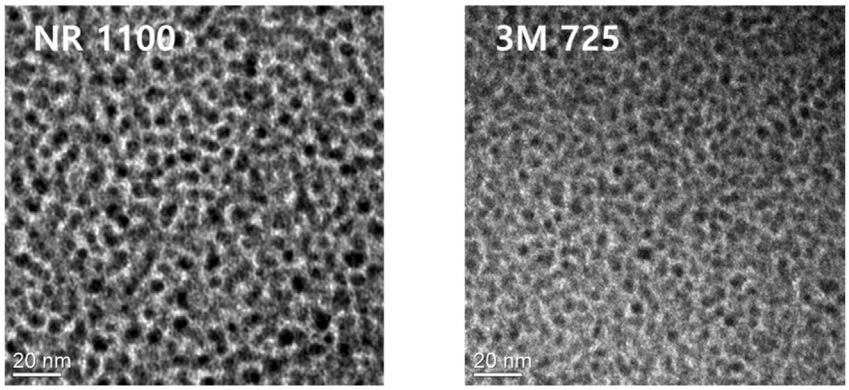

Fig. 4 – TEM images of NR 1100 and 3 M 725 membranes.

distributed. Moreover, it is interesting that the interdomain distance tends to be increased as a function of EW value of the SSC-PFSA ionomer membranes in the condition of possessing an identical chemical structure. A longer interdomain distance in the ionomer membrane would lead to a longer proton transport pathway, as protons in a hydrophilic domain move to an adjacent hydrophilic domain regardless of the assistance of water molecules.

Fig. 5 presents the proton conductivity of PFSA ionomer membranes that were examined by four-point probe alternating current (a. c.) impedance spectroscopy in water [36]. The proton conduction was increased as a function of temperature in all the PFSA ionomer membrane samples presumably due to the enhanced proton mobility. NR 1100 exhibited the minimum proton conductivity among all the PFSA ionomer membranes employed in this study. On the other hand, the SSC-PFSA membranes show relatively high proton conductivity values owing to their narrowly arranged morphological distribution. For the SSC-PFSA ionomer membranes with an identical chemical structure, both their EW values and interdomain distances significantly affect the proton conductivity. The proton conductivity values of 3 M 725 and AQ 720 exceeded those of 3 M 800 and AQ 790, respectively. These results suggest that the proton conductivity can be enhanced for the membranes with reduced EW values and shortened interdomain distance [56]. In contrast, 3 M 725 and 3 M 800 ionomer membranes that are characterized by a relatively higher EW value and a longer interdomain distance (3.13–3.16 nm) exhibited superior proton conductivity to that of AQ 720 ionomer membranes that possess a lower EW value and a shorter interdomain distance (3.12 nm). This unusual proton transport behavior can be justified by taking into account a correlation found between proton conductivity and membrane swelling in the fully hydrated state. In general, as the amount of water molecules absorbed into the membranes increases, the concentration of sulfonic acid groups per a unit volume of PFSA ionomer membranes decreases. This dilution

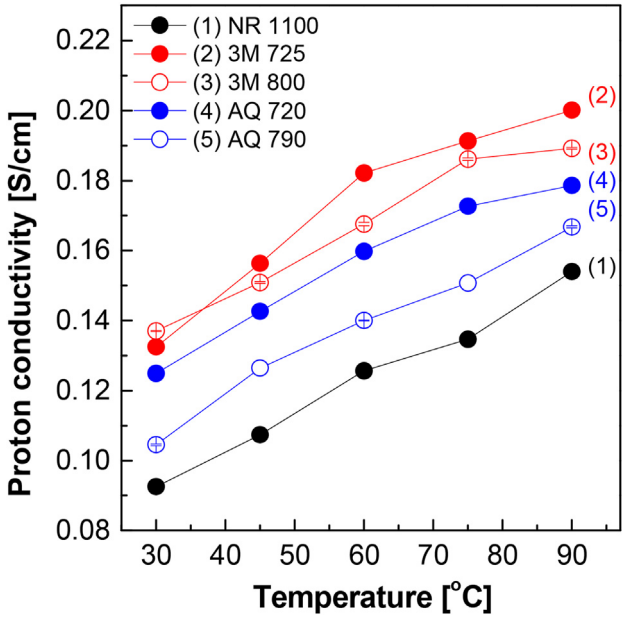

Fig. 5 – Proton conductivity of the PFSA membranes as a function of temperature.

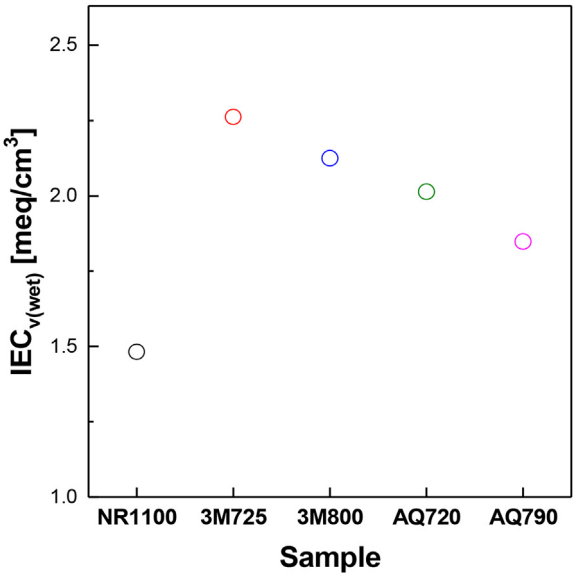

Fig. 6 – $IEC_{v(wet)}$ comparison in the PFSA ionomer membranes.

Table 3 – Fundamental PFSA ionomer membrane characteristics.

PFSA membrane	Density [g/cm^3]		Water uptake [%]	Tensile strength[a] [MPa]	T_α[b] [°C]
	Dry state	Wet state			
NR 1100	1.98	1.63	39.7	20.4 ± 0.4	104.9
3 M 725	2.09	1.64	31.7	23.2 ± 0.3	114.4
3 M 800	2.08	1.70	28.0	23.0 ± 0.3	113.1
AQ 720	2.01	1.45	41.4	13.8 ± 0.2	115.6
AQ 790	2.00	1.46	39.9	13.3 ± 0.5	104.9

[a] Obtained via conventional INSTRON measurement (Universal Testing Machine, UTM, T7000 M, crosshead speed = 10 mm/min, measurement temperature = 25 °C, humidity = 50% RH).
[b] Examined using dynamic mechanical analyzer (DMA, DMA 8000, Perkin Elmer Corp.) at a ramp speed of 5 °C/min under air atmosphere.

effect would decrease the overall proton conductivity in the PFSA ionomer membranes. Thus, it is more convenient to use the term of $IEC_{v(wet)}$ [meq/cm^3] that is defined as the ion exchange capacity per a unit volume of a membrane swollen in the fully hydrated state. When the EW values are similar, the shorter the side chain length, the lower the water absorption [57]. The $IEC_{v(wet)}$ value of AQ 720 is lower than that of 3 M ionomers (Fig. 6) although it achieves the minimum EW value and the shortest interdomain distance at a dried state. These results clearly support a higher water uptake of AQ 720 compared to others (Table 3). In the presence of an increased amount of absorbed water molecules, the proton concentration is diluted and, therefore, the proton conductivity is reduced [58,59]. Hence, maintaining an appropriate amount of water uptake in the ionomer membranes will lead to a regulation of the performance of proton conductivity [60,61].

3.5. *Gas barrier behavior*

A gas barrier property for H_2 has been confirmed as an another type of crucial characteristic of PEMEC membranes, which is inversely proportional to the gas permeability [52]. Fig. 7 illustrates the variations of H_2 and O_2 permeabilities of the PFSA ionomer membranes as a function of temperatures. Regardless of the type of feed gas, the gas permeability for all PFSA ionomer membranes increased at an elevated temperature. The extent of the H_2 permeation was much higher than that of O_2 permeation under an identical pressure condition. As the van der Waals volume (44.19 Å^3) of H_2 molecules is much smaller than that of O_2 molecules (Van der Waal volume = 52.86 Å^3), one can expect an easier diffusion of H_2 through the membranes [62]. Notice that the H_2 permeation behavior in the PFSA ionomer membranes shown in Fig. 7(a) can also be correlated to the average particle size of the ionomers dispersed in the aqueous medium; the H_2 permeability decreases as the average particle size decreases. For instance, NR 1100 that possesses the largest ionomer particle sizes exhibits the maximum H_2 permeability, whereas 3 M 725 and AQ 720 that possess relatively smaller ionomer dispersion particles exhibit a prominent H_2 barrier property. It can be concluded that generally smaller ionomer particles that are dispersed in solution can facilitate a formation of tightly packed membranes which can role as a better H_2 barrier [28].

Similar to the property found in the H_2 permeation behavior, the PFSA ionomer membranes with an identical chemical structure also demonstrates a correlation between the O_2 permeation behavior and the EW values (Fig. 7(b)). An ionomer with a high-EW value exhibits a higher permeability of O_2 than an ionomer with a low-EW value probably due to the presence of more hydrophobic segments in the high-EW ionomer [63]. An ionomer type with a higher EW value can offer higher free volumes that would be effectively used as pathways for the migration of gaseous molecules when compared to those present in the hydrophilic phase. On the other hand, the impact of side chain length is remarkable in SSC-PFSA ionomer membranes as O_2 barriers that the shorter C2 ionomers (AQ ionomers) are notably less permeable to the O_2 permeation than the longer C4 ionomers (3 M ionomers).

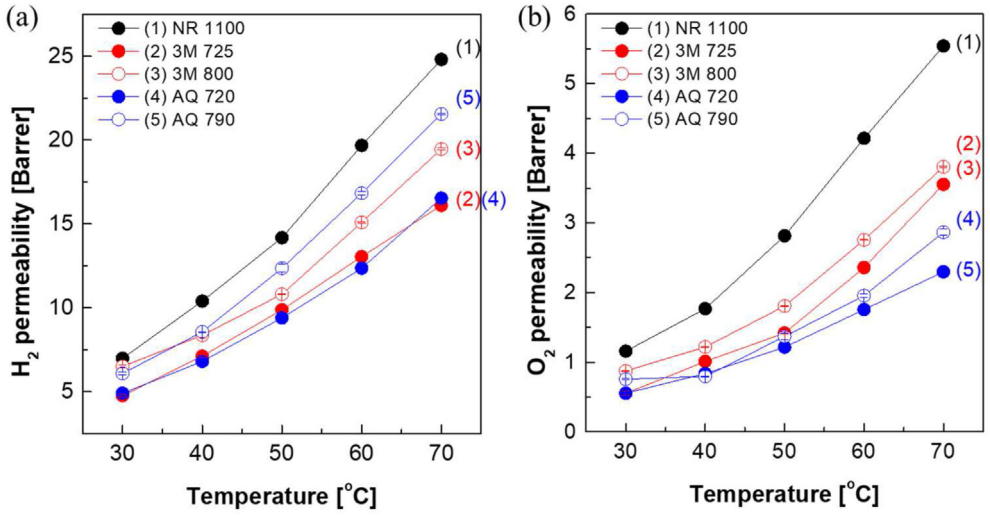

Fig. 7 – (a) H_2 and (b) O_2 permeability of PFSA ionomer membranes in the unit of barrer (10^{10} cm^3_{stp} cm/sec cm^2 cm Hg).

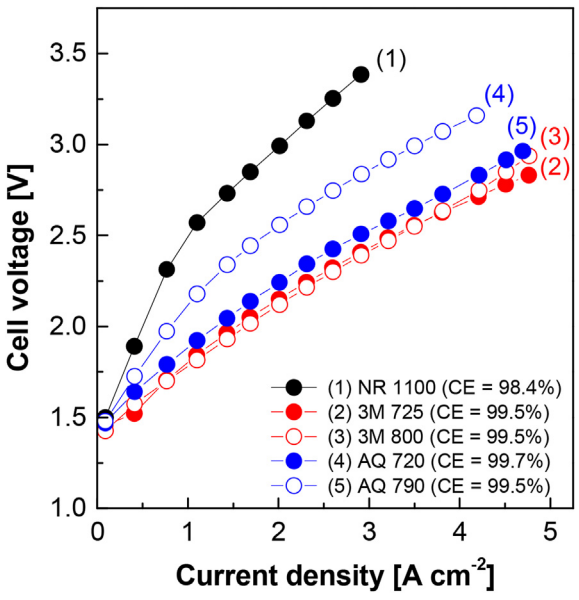

Fig. 8 – PEMEC single cell performance of the PFSA ionomer membranes examined at 80 °C.

3.6. *Electrochemical performance of PEMEC single cell*

Fig. 8 shows the electrochemical performance exhibited by PEMEC cells depending on the chemical structures and EW values of the PFSA ionomer membranes. Their open circuit voltage (OCV) values decrease as the function of the H_2 barrier property in the activation polarization region. The slopes in ohmic polarization region slow down as impedance values of the corresponding PFSA ionomer membranes become small or their proton conductivity values increase [64]. Consequently, 3 M 725 shows an excellent PEMEC performance due to the combinational effect of the relatively low H_2 permeability and the highest proton conductivity. Among the SSC-PFSA ionomer membranes, the PEMEC performance of AQ 720 was lower than that of 3 M 800. This is because O_2 barrier properties of AQ ionomer membranes are weakened because the H_2 pressure in cathodic side is much higher than the O_2 pressure in anodic side. Furthermore, 3 M ionomer membranes afford effective proton transport properties due to having a balanced concentration of sulfonic acid groups (i.e., $IEC_{v(wet)}$) under the PEMEC operation conditions. Note that all the SSC-PFSA ionomer membranes had almost similar current efficiency (CE).

4. Conclusion

The physicochemical properties of commercially available PFSA ionomer membranes were systematically investigated, considering their PEMEC membrane applications. The structural characteristics of the PFSA membranes were identified by the solid-state ^{19}F MAS NMR spectroscopy. As identified from the result of this study, 3 M ionomers and AQ ionomers possess C4 and C2 side chains onto the PTFE main backbones, respectively. All the PFSA ionomers exhibited thermal decomposition behaviors that can be correlated to 1) water evaporation, 2) desulfonation, and 3) thermal degradation of their side chains and main backbones. 3 M ionomers maintained a thermal resistance up to 250 °C different in other PFSA ionomers. The particle sizes in the dispersion state play a critical role in determining H_2 gas barrier properties. To be more specific, the H_2 permeability tended to be decreased in the membranes due to the gradual decrease in the size of ionomer particles in the dispersion state. The proton conductivity was enhanced in the PFSA ionomer membranes with a decreased EW value even in the presence of an identical chemical structure. Smaller ionomer particles typically make a narrow average packing distance in the hydrophilic domains and are well distributed throughout the PFSA membrane. This morphological characteristic may be a benefit in creating faster proton transport pathways. 3 M ionomer membranes with relatively high EW values have exhibited superior proton conductivity over the AQ 720 membranes with the low EW values. This result might be attributed to the excessive water swelling of AQ 720, lowering the concentration of sulfonic acid groups in the hydrated state. Upon application to PEMEC, the single cell performance of the PFSA ionomer membranes was comprehensively influenced by both proton conductivity as well as the H_2 permeability across the PFSA membranes. Consequently, 3 M 725 exhibited the highest PEMEC performance due to a synergistic effect of the proton conduction and H_2 gas barrier property.

Declaration of competing interest

The authors declare that they have no known competing financial interests or personal relationships that could have appeared to influence the work reported in this paper.

Acknowledgment

We thank Dr. Denis Duchesne and Dr. Lisa Chen of 3 M Advanced Materials Division for ionomer material supply and technical support. This work was supported by the Korea Institute of Energy Technology Evaluation and Planning (KETEP) grant funded by the Korea government (MOTIE) (RS-2023-00241035, Clean Hydrogen and Ammonia Innovation Research Center). This work was also supported by the Technology Innovation Program (1415186266/20012133) funded By the Ministry of Trade, Industry & Energy (MOTIE, Korea) and the Korea Evaluation Institute of Industrial Technology (KEIT). SW acknowledges the support of the National High Magnetic Field Laboratory, which is funded by National Science Foundation Cooperative Agreement No. DMR-2128556 and the State of Florida.

REFERENCES

[1] Züttel A. Hydrogen storage methods. Naturwissenschaften 2004;91:157–72.
[2] Chisholm G, Cronin L. Chapter 16 - hydrogen from water electrolysis. In: Letcher TM, editor. Storing energy. Oxford: Elsevier; 2016. p. 315–43.

[3] Gregory DP, Ng DYC, Long GM. The hydrogen economy. In: Bockris JOM, editor. Electrochemistry of cleaner environments. Boston, MA: Springer US; 1972. p. 226–80.
[4] Ball M, Wietschel M. The future of hydrogen – opportunities and challenges. Int J Hydrogen Energy 2009;34:615–27.
[5] De Angelis S, Schuler T, Sabharwal M, Holler M, Guizar-Sicairos M, Müller E, et al. Understanding the microstructure of a core–shell anode catalyst layer for polymer electrolyte water electrolysis. Sci Rep 2023;13:4280.
[6] Rosli RE, Sulong AB, Daud WRW, Zulkifley MA, Husaini T, Rosli MI, et al. A review of high-temperature proton exchange membrane fuel cell (HT-PEMFC) system. Int J Hydrogen Energy 2017;42:9293–314.
[7] Chandan A, Hattenberger M, El-kharouf A, Du S, Dhir A, Self V, et al. High temperature (HT) polymer electrolyte membrane fuel cells (PEMFC) – a review. J Power Sources 2013;231:264–78.
[8] Winter C-J. Hydrogen energy — abundant, efficient, clean: a debate over the energy-system-of-change. Int J Hydrogen Energy 2009;34:S1–52.
[9] Agnolucci P, Akgul O, McDowall W, Papageorgiou LG. The importance of economies of scale, transport costs and demand patterns in optimising hydrogen fuelling infrastructure: an exploration with SHIPMod (Spatial hydrogen infrastructure planning model). Int J Hydrogen Energy 2013;38:11189–201.
[10] Abdol Rahim AH, Tijani AS, Kamarudin SK, Hanapi S. An overview of polymer electrolyte membrane electrolyzer for hydrogen production: modeling and mass transport. J Power Sources 2016;309:56–65.
[11] Armaroli N, Balzani V. The hydrogen issue. ChemSusChem 2011;4:21–36.
[12] Najjar YSH. Hydrogen safety: the road toward green technology. Int J Hydrogen Energy 2013;38:10716–28.
[13] Hamrock SJ, Yandrasits MA. Proton exchange membranes for fuel cell applications. J Macromol Sci, Part C 2006;46:219–44.
[14] Carmo M, Fritz DL, Mergel J, Stolten D. A comprehensive review on PEM water electrolysis. Int J Hydrogen Energy 2013;38:4901–34.
[15] Rodgers MP, Bonville LJ, Kunz HR, Slattery DK, Fenton JM. Fuel cell perfluorinated sulfonic acid membrane degradation correlating accelerated stress testing and lifetime. Chem Rev 2012;112:6075–103.
[16] Collier A, Wang H, Zi Yuan X, Zhang J, Wilkinson DP. Degradation of polymer electrolyte membranes. Int J Hydrogen Energy 2006;31:1838–54.
[17] Banerjee S, Curtin DE. Nafion® perfluorinated membranes in fuel cells. J Fluor Chem 2004;125:1211–6.
[18] Trinke P, Keeley GP, Carmo M, Bensmann B, Hanke-Rauschenbach R. Elucidating the effect of mass transport resistances on hydrogen crossover and cell performance in PEM water electrolyzers by varying the cathode ionomer content. J Electrochem Soc 2019;166:F465.
[19] Xing Y, Li H, Avgouropoulos G. Research progress of proton exchange membrane failure and mitigation strategies. Materials 2021;14:2591.
[20] Curtin DE, Lousenberg RD, Henry TJ, Tangeman PC, Tisack ME. Advanced materials for improved PEMFC performance and life. J Power Sources 2004;131:41–8.
[21] Luo X, Holdcroft S, Mani A, Zhang Y, Shi Z. Water, proton, and oxygen transport in high IEC, short side chain PFSA ionomer membranes: consequences of a frustrated network. Phys Chem Chem Phys 2011;13:18055–62.
[22] Chen Q, Schmidt-Rohr K. ^{19}F and ^{13}C NMR signal assignment and analysis in a perfluorinated ionomer (nafion) by two-dimensional solid-state NMR. Macromolecules 2004;37:5995–6003.
[23] Blümich B. Introduction to compact NMR: a review of methods. TrAC, Trends Anal Chem 2016;83:2–11.
[24] Kavun VY, Uvarov NF, Merkulov EB, Polyantsev MM, Ulihin AS, Goncharuk VK, et al. Ion mobility and conductivity in fluorite-type solid solutions in the KF–MF_2–BiF_3 systems (M=Ba, Cd) according to ^{19}F NMR and conductivity data. Solid State Ionics 2015;274:4–7.
[25] Kusoglu A, Weber AZ. New insights into perfluorinated aulfonic-acid ionomers. Chem Rev 2017;117:987–1104.
[26] Safronova EY, Voropaeva DY, Safronov DV, Stretton N, Parshina AV, Yaroslavtsev AB. Correlation between Nafion morphology in various dispersion liquids and properties of the cast membranes. Membr 2023;13:13.
[27] Ahn C-Y, Ahn J, Kang SY, Kim O-H, Lee DW, Lee JH, et al. Enhancement of service life of polymer electrolyte fuel cells through application of nanodispersed ionomer. Sci Adv 2020;6:eaaw0870.
[28] Ahn J, Ali MI, Lim JH, Park Y, Park IK, Duchesne D, et al. Highly dispersed CeOx hybrid nanoparticles for perfluorinated sulfonic acid ionomer–poly(tetrafluoethylene) reinforced membranes with improved service life. Membr 2021;11:143.
[29] Dai Z, Ansaloni L, Deng L. Recent advances in multi-layer composite polymeric membranes for CO2 separation: a review. Green Energy Environ 2016;1:102–28.
[30] Shin S-H, Nur PJ, Kodir A, Kwak D-H, Lee H, Shin D, et al. Improving the mechanical durability of short-side-chain perfluorinated polymer electrolyte membranes by annealing and physical reinforcement. ACS Omega 2019;4:19153–63.
[31] Sumner MJ, Harrison WL, Weyers RM, Kim YS, McGrath JE, Riffle JS, et al. Novel proton conducting sulfonated poly(arylene ether) copolymers containing aromatic nitriles. J Membr Sci 2004;239:199–211.
[32] Park CH, Lee CH. Disulfonated copolyimide-boehmite nanocomposite fuel cell membranes with improved chemical resistance. Macromol Res 2015;23:45–52.
[33] Lee CH, Lee K-S, Lane O, McGrath JE, Chen Y, Wi S, et al. Solvent-assisted thermal annealing of disulfonated poly(arylene ether sulfone) random copolymers for low humidity polymer electrolyte membrane fuel cells. RSC Adv 2012;2:1025–32.
[34] Page KA, Landis FA, Phillips AK, Moore RB. SAXS analysis of the thermal relaxation of anisotropic morphologies in oriented nafion membranes. Macromolecules 2006;39:3939–46.
[35] Kwang-Woo K, Jehan K, Young Duck Y, Hyungju A, Byoungseok M, Na Hyung K, et al. Small-angle X-ray scattering beamline BL4C SAXS at Pohang light source II. Biodesign 2017;5:24–9.
[36] Lee CH, Park HB, Lee YM, Lee RD. Importance of proton conductivity measurement in polymer electrolyte membrane for fuel cell application. Ind Eng Chem Res 2005;44:7617–26.
[37] Kim DS, Robertson GP, Kim YS, Guiver MD. Copoly(arylene ether)s containing pendant sulfonic acid groups as proton exchange membranes † NRCC publication No. 50899. Macromolecules 2009;42:957–63.
[38] Kim YS, Pivovar BS. Moving beyond mass-based parameters for conductivity analysis of sulfonated polymers. Annu Rev Chem Biomol Eng 2010;1:123–48.
[39] Hou J, Jang W, Kim S, Kim J-H, Byun H. Rapid formation of polyimide nanofiber membranes via hot-press treatment and their performance as Li-ion battery separators. RSC Adv 2018;8:14958–66.
[40] Emery M, Frey M, Guerra M, Haugen G, Hintzer K, Lochhaas KH, et al. The development of new membranes for proton exchange membrane fuel cells. ECS Trans 2007;11:3.
[41] Schaberg MS, Abulu JE, Haugen GM, Emery MA, O'Conner SJ, Xiong PN, et al. New multi acid side-chain ionomers for

proton exchange membrane fuel cells. ECS Trans 2010;33:627.
[42] Wu H, Kruczek B, Thibault J. Impact of measuring devices and data analysis on the determination of gas membrane properties. J Memb Sci Res 2018;4:4–14.
[43] Rutherford SW, Do DD. Review of time lag permeation technique as a method for characterisation of porous media and membranes. Adsorption 1997;3:283–312.
[44] Stern SA. The "barrer" permeability unit. J Polym Sci 2 Polym Phys 1968;6:1933–4.
[45] Robert M, Kaddouri AE, Perrin J-C, Leclerc S, Lottin O. Towards a NMR-based method for characterizing the degradation of nafion XL membranes for PEMFC. J Electrochem Soc 2018;165:F3209.
[46] Ghassemzadeh L, Kreuer KD, Maier J, Müller K. Evaluating chemical degradation of proton conducting perfluorosulfonic acid ionomers in a Fenton test by solid-state ^{19}F NMR spectroscopy. J Power Sources 2011;196:2490–7.
[47] Yan ZB, Hayes R, Melo LGA, Goward GR, Hitchcock AP. X-Ray absorption and solid-state NMR spectroscopy of fluorinated proton conducting polymers. J Phys Chem C 2018;122:3233–44.
[48] Yan ZB, Brouwer DH, Goward GR. 19F double quantum NMR spectroscopy: a tool for probing dynamics in proton-conducting fluorinated polymer materials. Macromolecules 2016;49:7331–9.
[49] de Almeida S, Kawano Y. Thermal behavior of nafion membranes. J Therm Anal Calorim 1999;58:569–77.
[50] Feng M, Qu R, Wei Z, Wang L, Sun P, Wang Z. Characterization of the thermolysis products of Nafion membrane: a potential source of perfluorinated compounds in the environment. Sci Rep 2015;5:9859.
[51] Kim OH, Oh SH, Ahn CY, Kim S, Kim JK, Kim J, et al. Enhanced performance of ionomer binder with shorter side-chains, higher dispersibility, and lower equivalent weight. Fuel Cell 2018;18:711–22.
[52] Schalenbach M, Carmo M, Fritz DL, Mergel J, Stolten D. Pressurized PEM water electrolysis: efficiency and gas crossover. Int J Hydrogen Energy 2013;38:14921–33.
[53] Kusoglu A, Hexemer A, Jiang R, Gittleman CS, Weber AZ. Effect of compression on PFSA-ionomer morphology and predicted conductivity changes. J Membr Sci 2012;421–422:283–91.
[54] Mochizuki T, Kakinuma K, Uchida M, Deki S, Watanabe M, Miyatake K. Temperature- and humidity-controlled SAXS analysis of proton-conductive ionomer membranes for fuel cells. ChemSusChem 2014;7:729–33.
[55] Hwang JP, Park IK, Park CH, Lee CH. Morphological transformation of perfluorinated sulfonic acid ionomer via ionic complex formation at a high entropy state. Mater Today Energy 2023;33:101250.
[56] Lim JH, Hou J, Lee CH. Dynamic mechanical fatigue behavior of polymer electrolyte membranes for fuel cell electric vehicles using a gas pressure-loaded blister. Polymers 2021;13:4177.
[57] Li J, Pan M, Tang H. Understanding short-side-chain perfluorinated sulfonic acid and its application for high temperature polymer electrolyte membrane fuel cells. RSC Adv 2014;4:3944–65.
[58] Park CH, Lee CH, Guiver MD, Lee YM. Sulfonated hydrocarbon membranes for medium-temperature and low-humidity proton exchange membrane fuel cells (PEMFCs). Prog Polym Sci 2011;36:1443–98.
[59] Lee CH, Park HB, Chung YS, Lee YM, Freeman BD. Water sorption, proton conduction, and methanol permeation properties of sulfonated polyimide membranes cross-linked with N,N-Bis(2-hydroxyethyl)-2-aminoethanesulfonic acid (BES). Macromolecules 2006;39:755–64.
[60] Schiavone M-M, Zhao Y, Iwase H, Arima-Osonoi H, Takata S-i, Radulescu A. On the proton conduction pathways in polyelectrolyte membranes based on syndiotactic-polystyrene. Membranes 2022;12:143.
[61] Shi S, Weber AZ, Kusoglu A. Structure-transport relationship of perfluorosulfonic-acid membranes in different cationic forms. Electrochim Acta 2016;220:517–28.
[62] Bondi A. van der Waals volumes and radii. J Phys Chem 1964;68:441–51.
[63] Takeuchi K, Kuo A-T, Hirai T, Miyajima T, Urata S, Terazono S, et al. Hydrogen permeation in hydrated perfluorosulfonic acid polymer membranes: effect of polymer crystallinity and equivalent weight. J Phys Chem C 2019;123:20628–38.
[64] Tijani AS, Ghani MFA, Rahim AHA, Muritala IK, Binti Mazlan FA. Electrochemical characteristics of (PEM) electrolyzer under influence of charge transfer coefficient. Int J Hydrogen Energy 2019;44:27177–89.